Integrative transcriptome sequencing identifies *trans*-splicing events with important roles in human embryonic stem cell pluripotency

Chan-Shuo Wu,[1,3] Chun-Ying Yu,[2,3] Ching-Yu Chuang,[2] Michael Hsiao,[1]
Cheng-Fu Kao,[2] Hung-Chih Kuo,[2,4] and Trees-Juen Chuang[1,4]

[1]*Genomics Research Center, Academia Sinica, Taipei 11529, Taiwan;* [2]*Institute of Cellular and Organismic Biology, Academia Sinica, Taipei 11529, Taiwan*

***Trans*-splicing is a post-transcriptional event that joins exons from separate pre-mRNAs. Detection of *trans*-splicing is usually severely hampered by experimental artifacts and genetic rearrangements. Here, we develop a new computational pipeline, TSscan, which integrates different types of high-throughput long-/short-read transcriptome sequencing of different human embryonic stem cell (hESC) lines to effectively minimize false positives while detecting *trans*-splicing. Combining TSscan screening with multiple experimental validation steps revealed that most chimeric RNA products were platform-dependent experimental artifacts of RNA sequencing. We successfully identified and confirmed four *trans*-spliced RNAs, including the first reported *trans*-spliced large intergenic noncoding RNA ("ts*RMST*"). We showed that these *trans*-spliced RNAs were all highly expressed in human pluripotent stem cells and differentially expressed during hESC differentiation. Our results further indicated that ts*RMST* can contribute to pluripotency maintenance of hESCs by suppressing lineage-specific gene expression through the recruitment of NANOG and the PRC2 complex factor, SUZ12. Taken together, our findings provide important insights into the role of *trans*-splicing in pluripotency maintenance of hESCs and help to facilitate future studies into *trans*-splicing, opening up this important but understudied class of post-transcriptional events for comprehensive characterization.**

[Supplemental material is available for this article.]

Alternative splicing, which arises from post-transcriptional events, can lead to the generation of multiple transcript isoforms from a single gene, thus providing an essential source of diversity for the transcriptome and proteome (Graveley 2001; Maniatis and Tasic 2002; Black and Grabowski 2003; Bracco and Kearsey 2003; Blencowe 2006; Chen et al. 2006; Ben-Dov et al. 2008; Huang et al. 2008; Jin et al. 2008; Mudge et al. 2011). Splicing can occur either in *cis* or in *trans* (Horiuchi and Aigaki 2006; Gingeras 2009). *Cis*-splicing joins exons within a single precursor mRNA (pre-mRNA), whereas *trans*-splicing joins exons from two or more separate pre-mRNAs originating from the same gene (intragenic *trans*-splicing) or two or more different genes (intergenic *trans*-splicing). The best-characterized form of *trans*-splicing is spliced-leader (SL) *trans*-splicing, which provides mRNAs with a new 5′ cap and leader sequence, and commonly occurs in unicellular organisms, nematodes, and trypanosomes (Sutton and Boothroyd 1986; Krause and Hirsh 1987; Nilsen 2001; Hastings 2005). However, the mechanisms underlying non-SL *trans*-splicing remain largely unknown (Lasda and Blumenthal 2011). To date, only a few non-SL *trans*-splicing events have been well-documented. In higher eukaryotes, the best-known *trans*-splicing examples are two *Drosophila* genes, *mod*(*mdg4*) and *lola*, which are involved in apoptosis and axon guidance decisions, respectively (Dorn and Krauss 2003; Goeke et al. 2003). The most prominent examples of human genes that undergo *trans*-splicing reported so far are *JAZF1*-*SUZ12* (also known as *JJAZ1*) and *SLC45A3*-*ELK4*; the former is translated into a chimeric protein with anti-apoptotic function and is believed to be a prerequisite for chromosomal exchange (Li et al. 2008; Gingeras 2009; Schoenfelder et al. 2010), and the latter is related to prostate cancer (Gingeras 2009; Rickman et al. 2009). Although *trans*-splicing remains an understudied class of post-transcriptional events in higher eukaryotes, accumulating evidence suggests it is of biological significance (Gingeras 2009).

Generally, *trans*-splicing is detected by comparing the reference genomes with ESTs/mRNAs (Shao et al. 2006; Li et al. 2009; Herai and Yamagishi 2010; Kim et al. 2010) or by next-generation sequencing (NGS) of mRNAs (RNA-seq) (McManus et al. 2010; Zhang et al. 2010; Al-Balool et al. 2011; Fang et al. 2012). *Trans*-splicing events detected by such means may, however, include a considerable number of false positives that arise from experimental artifacts, such as template switching (McManus et al. 2010; Ozsolak and Milos 2011). Template switching is generated during RT-PCR and frequently emerges in cDNA products (Cocquet et al. 2006; Houseley and Tollervey 2010). A prominent study using hybrid mRNAs (i.e., *Drosophila melanogaster* females vs. *Drosophila sechellia* males) demonstrated that experimental artifacts are the predominant source of apparent *trans*-spliced RNA products observed in mRNA (McManus et al. 2010). It would, however, be impossible to apply such a system to humans. Furthermore, genetic rearrangements can form noncolinear (or chimeric) RNAs (Shao et al. 2006; Gingeras 2009; Frenkel-Morgenstern et al. 2012),

[3]**These authors contributed equally to this work.**
[4]**Corresponding authors**
E-mail kuohuch@gate.sinica.edu.tw
E-mail trees@gate.sinica.edu.tw

Article published online before print. Article, supplemental material, and publication date are at http://www.genome.org/cgi/doi/10.1101/gr.159483.113. Freely available online through the *Genome Research* Open Access option.

© 2014 Wu et al. This article, published in *Genome Research*, is available under a Creative Commons License (Attribution-NonCommercial 3.0 Unported), as described at http://creativecommons.org/licenses/by-nc/3.0/.

which are not easily distinguished from *trans*-spliced RNAs, presenting another challenge to the accurate detection of *trans*-splicing. To our knowledge, there is currently no available method of systematically analyzing *trans*-splicing that can simultaneously account for experimental artifacts and genetic rearrangements in humans.

To address these issues, we developed TSscan, which utilizes transcriptome sequencing data from different NGS platforms and different undifferentiated human embryonic stem cell (hESC) lines. It is important to note that hESCs have been reported to have a very high level of transcriptome complexity, and high transcript diversity has been suggested to contribute to hESC pluripotency (Wu et al. 2010). As such, it is worth investigating whether *trans*-splicing exists and is biologically significant in hESCs. By performing TSscan screening combined with multiple experimental validation steps, we successfully confirmed that four *trans*-splicing events occur in hESCs. We found that these *trans*-spliced RNAs were all highly expressed in human pluripotent stem cells and differentially expressed during hESC differentiation. We also identified the first *trans*-spliced large intergenic noncoding RNA, showed that it tends to be specifically transcribed in human pluripotent stem cells, and significantly affects pluripotency maintenance of hESCs. Therefore, this study not only describes a new approach to systematically detect *trans*-splicing, but also provides further insight into the potential roles of *trans*-splicing in hESC pluripotency and early human embryonic development.

Results

Identification of *trans*-spliced RNAs in hESCs using TSscan

To search for *trans*-splicing events in hESCs, we generated 0.83 million long reads (averaging 353.7 bp) and 230.63 million short reads (50 bp) from H9 hESCs by performing Roche 454 and SOLiD whole-transcriptome sequencing, respectively, and directly downloaded the 454/Illumina RNA-seq data of H1 hESCs from a publicly available database (Table 1; Wu et al. 2010). Since *trans*-splicing may also join colinear exons such as *mod*(*mdg4*) and *lola* (Dorn and Krauss 2003; Goeke et al. 2003), in this study we only consider *trans*-spliced noncolinear (or chimeric) RNA candidates for simplicity. TSscan involved four main screening steps (Fig. 1A). First, we searched for all possible chimeric RNA candidates by aligning the long 454 reads of hESC H1/H9 against the human reference genome (see Methods) and extracted 8822 candidates (Fig. 1B). The junction sites between two topologically distinct genomic loci were designated as "chimeric junction sites." Of note, since both 454 RNA-seq libraries were prepared by oligo-dT selection, the retrieved chimeric RNA candidates are unlikely to be noncolinearly encoded RNAs that were *cis*-spliced to form circular RNAs (i.e., RNAs in which the exon order is a circular permutation of that encoded by the corresponding genomic sequence [Hsu and Coca-Prados 1979; Nigro et al. 1991]). Second, to minimize the possibility of false positives resulting from lack of depth in long reads or NGS platform specificity, we aligned the short reads (i.e., SOLiD/Illumina reads) against the 8822 long-read-nominated candidates and discarded the candidates that were not supported by short reads. The remaining candidates were then categorized into four subsets according to the types of supporting RNA-seq data (i.e., S1–S4; see Fig. 1B). Third, to further eliminate potential experimental artifacts, candidates that satisfied any of the following in silico filters were eliminated: (1) chimeric junction sites containing short homologous sequences (SHSs) or gaps (as these tend to arise from template switching) (McManus et al. 2010); (2) sense–antisense fusion candidates containing noncanonical splicing signals at the chimeric junction sites (Houseley and Tollervey 2010); and (3) candidates containing sequences from the mitochondrial genome (McManus et al. 2010). Finally, to eliminate potential genetic rearrangements, only the nine candidates that were supported by RNA-seq data from both H1 and H9 hESCs were retained (Fig. 1B; Table 2). Upon completion of the TSscan screening process, ~99.9% of the 454-nominated candidates had been discarded. We reason that the presence of experimental artifacts is the most likely explanation for the TSscan-excluded cases (see Discussion).

Experimental validation of *trans*-splicing events identified by TSscan

To confirm that the nine candidates identified by TSscan were indeed examples of *trans*-splicing, we designed a series of experimental validations (Fig. 1A). We first performed RT-PCR with Moloney Murine Leukemia Virus (MMLV)-derived reverse transcriptase (RTase) (the NGS cDNA library was generated using the same RTase), and found that the transcripts of five *trans*-splicing candidates were readily detected in multiple hESC lines (H1, H9, and NTU1) (Fig. 1C). These transcripts were not detected in the RT-free control, establishing that they did not arise from genomic contamination (Fig. 1C). As the chimeric junction sites of these five cases are all intragenic (originating from *CSNK1G3*, *ARHGAP5*, *FAT1*, *RMST*, and *SOBP*), they are designated as ts*CSNK1G3*, ts*ARHGAP5*, ts*FAT1*, ts*RMST*, and ts*SOBP*, respectively. False positive splicing events that arise from template switching tend to be RTase-dependent and can therefore be detected by comparing the PCR products that arise from the products of different RTases (Houseley and Tollervey 2010). As such, we further validated the five cases by RT-PCR using Avian Myeloblastosis Virus (AMV)-derived RTase. This revealed that ts*SOBP* is MMLV-RTase-dependent, and thus an artifact (Fig. 1D). Increasing the primer annealing temperature of MMLV-based RTase experiments has been previously shown to suppress the occurrence of template switching (Ouhammouch and Brody 1992; Cocquet et al. 2006); however, we found that increasing the temperature did not eliminate the ts*SOBP* artifact (Supplemental Fig. 1). We further examined these five cases by performing RNase protection assay (RPA; Supplemental Material), a non-RTase-based validation of RNA (Djebali et al. 2012), on total RNA of hESC H9, and found that only the probes for the RTase dependent-case ts*SOBP* were degraded (Supplemental Fig. 2). These results indicated that ts*SOBP* was indeed an experimental artifact. We thus emphasize the necessity of comparing the products of different RTases in confirming *trans*-splicing. Finally, we used qRT-PCR to show that *trans*-splicing was not a rare event in hESCs (Fig. 1E), and sequenced the RT-PCR amplicons to validate the identity of the chimeric junction sites

Table 1. NGS data sets used in this study

NGS platform		hESC lines	Number of reads	Length (bp)
Long reads	Roche 454	H1[a]	1,545,096	235.9 (average)
		H9	832,438	353.7 (average)
Short reads	Illumina GA II	H1[a]	132,455,091	27–36
	SOLiD	H9	230,632,477	50

[a]The NGS data were downloaded from the Gene Expression Omnibus (GEO; http://www.ncbi.nlm.nih.gov/geo/) (accession number GSE20301).

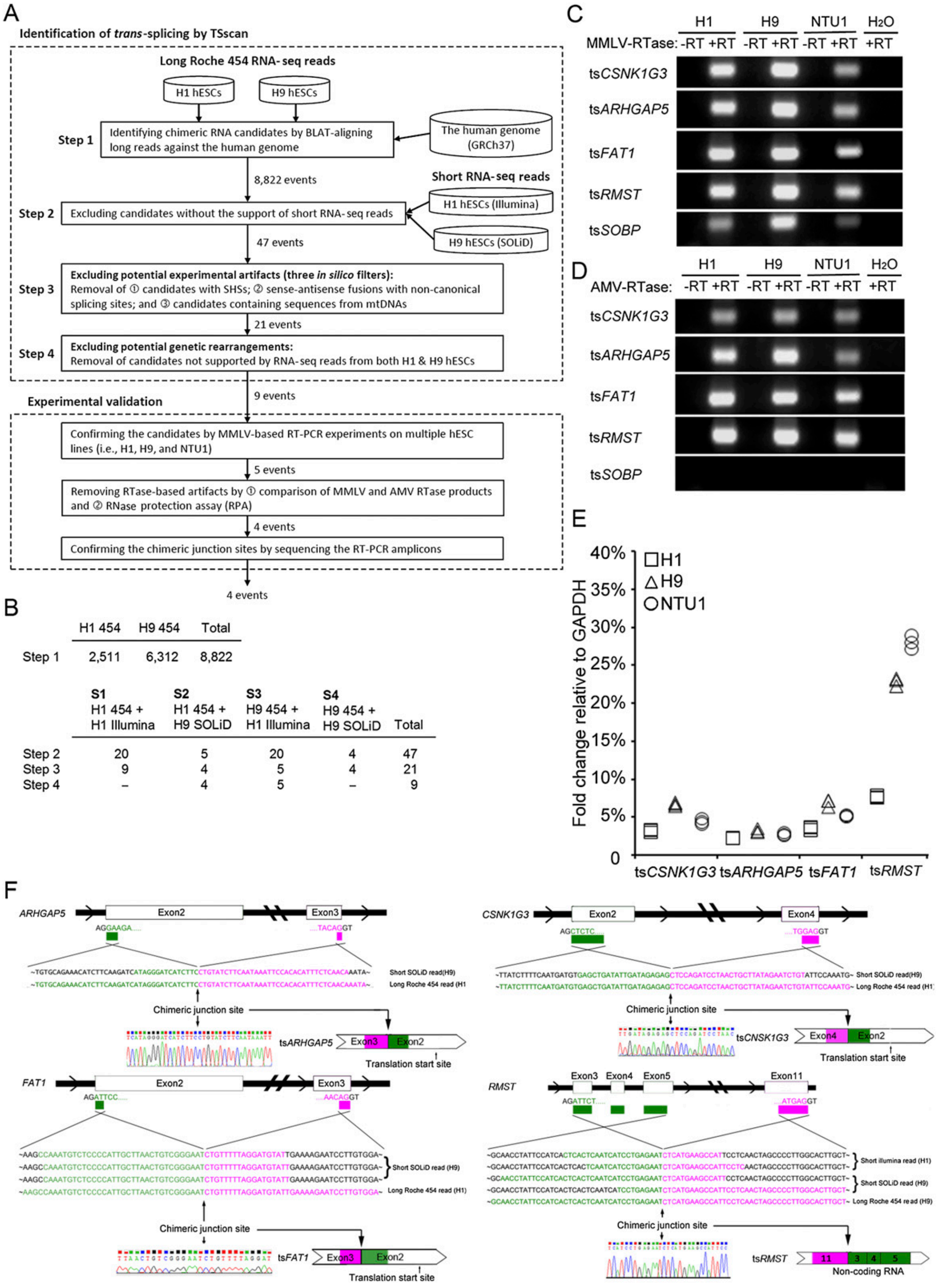

	H1 454	H9 454	Total
Step 1	2,511	6,312	8,822

	S1 H1 454 + H1 Illumina	S2 H1 454 + H9 SOLiD	S3 H9 454 + H1 Illumina	S4 H9 454 + H9 SOLiD	Total
Step 2	20	5	20	4	47
Step 3	9	4	5	4	21
Step 4	–	4	5	–	9

Figure 1. Identification and experimental validation of *trans*-splicing events in the transcriptome of hESCs. (*A*) TSscan identification and subsequent experimental validation. TSscan identification involved four steps. The first three steps identified *trans*-spliced RNA candidates and removed potential in vitro artifacts, and the last step removed potential genetic rearrangements. (SHS) Short homologous sequences. (*B*) The number of candidates remaining after each TSscan filter step. Note that one candidate may simultaneously belong to different data sets. For example, in Step 2, one candidate belongs to both S1 and S2, and one candidate belongs to both S3 and S4. (*C*) MMLV-RTase-based and (*D*) AMV-RTase-based RT-PCR products of ts*CSNK1G3*, ts*ARHGAP5*, ts*FAT1*, ts*RMST*, and ts*SOBP* in three types of hESC line (H1, H9, and NTU1). (±RT) RT-PCR without/with RTase. (*E*) qRT-PCR analysis of ts*CSNK1G3*, ts*ARHGAP5*, ts*FAT1*, and ts*RMST* in multiple hESC lines (H1, H9, and NTU1). (*F*) Schematic representations (*top*) and sequence chromatograms (*bottom*) for ts*CSNK1G3*, ts*ARHGAP5*, ts*FAT1*, and ts*RMST*. The long/short RNA-seq reads that support the chimeric junction sites (indicated by arrows) of the corresponding *trans*-spliced RNAs are shown.

Table 2. Nine *trans*-spliced RNA candidates identified by TSscan

Loci	Supported NGS platforms and hESC lines	Number of supported reads (long/short)	Splicing signals at the junction sites	Fusion type	AMV-based validation
CSNK1G3 (e4–e2)	H1 454, H9 SOLiD	2 (1/1)	Canonical	Intragenic	Pass
ARHGAP5 (e3–e2)	H1 454, H9 SOLiD	2 (1/1)	Canonical	Intragenic	Pass
FAT1 (e3–e2)	H1 454, H9 SOLiD	4 (1/3)	Canonical	Intragenic	Pass
RMST (e11–e3)	H9 454, H9 SOLiD, H1 Illumina	5 (1/4)	Canonical	Intragenic	Pass
SOBP (e3–e2)	H1 454, H9 SOLiD	10 (1/9)	Canonical	Intragenic	Fail
NCL (e3–e3)	H9 454, H1 Illumina	2 (1/1)	Noncanonical	Intragenic	Fail
USMG5–NBR1	H9 454, H1 Illumina	2 (1/1)	Noncanonical	Intergenic	Fail
18q23.3–12q14.2	H9 454, H1 Illumina	4 (1/3)	Noncanonical	Intergenic	Fail
1q21.2–1q21.1	H9 454, H1 Illumina	5 (1/4)	Noncanonical	Uncertain[a]	Fail

(e) Exon.
[a]Both chimeric regions of the *trans*-splicing candidate are in physical proximity on the same chromosome and are located in unannotated regions.

(Fig. 1F). Collectively, the preceding results provide multiple lines of evidence in support of the four candidates being genuine *trans*-spliced transcripts.

Although ts*ARHGAP5* was previously detected in tumors (Al-Balool et al. 2011), these four RNAs have not been reported to be expressed in hESCs. For ts*CSNK1G3*, ts*ARHGAP5*, and ts*FAT1*, *trans*-splicing was found to occur in the 5′ UTR upstream of the start codon (Fig. 1F). Of special significance is the identity of *RMST* as a large intergenic noncoding RNA (lincRNA) (Chan et al. 2002). As examined by the coding potential calculator (score < 53) (Kong et al. 2007), ts*RMST* is the first *trans*-spliced lincRNA to be identified through multiple experimental validations.

Trans-spliced RNAs are differentially expressed during hESC differentiation

We proceeded to examine whether the four transcripts identified in hESCs are also expressed in human induced pluripotent stem cells (iPSCs) reprogrammed from various somatic cell types, including skin fibroblast, dermal papilla cells, and granulose cells (Huang et al. 2010). As shown in Figure 2A, all four *trans*-spliced RNAs were expressed in each tested human iPSC clone, suggesting that these events tend to occur in human pluripotent stem cells. We then examined whether expression of these *trans*-spliced transcripts is associated with differentiation status by comparing their expression levels between undifferentiated and differentiated hESCs. We observed that ts*CSNK1G3*, ts*ARHGAP5*, and ts*FAT1* exhibited elevated expression levels upon in vitro differentiation, whereas the expression level of ts*RMST* was significantly decreased after in vitro differentiation (Fig. 2B). These results revealed that these *trans*-spliced transcripts were differentially expressed during hESC in vitro differentiation, indicating that they may play significant roles in pluripotency-related regulation or pathways regulating early lineage differentiation.

Furthermore, we compared the expression of each *trans*-spliced isoform with that of its corresponding colinear isoform in pluripotent stem cells. We first performed qRT-PCR analysis to examine the expression levels of each type of isoform in multiple hESC lines (H1, H9, and NTU1) and iPSCs (iGra2, iCFB50, and iCD3). In pluripotent stem cells, the expression level of ts*RMST* was remarkably higher than *RMST*, whereas similar or lower expression levels were observed between the other three *trans*-spliced transcripts and their respective colinear counterparts (Supplemental Fig. 3). We then examined the expression profiles of these two types of isoforms by RT-PCR (Fig. 2C) and qRT-PCR (Supplemental Fig. 4) in ten human normal tissues. We found that although ts*CSNK1G3*, ts*ARHGAP5*, and ts*FAT1* were also expressed in somatic cells, they were expressed in fewer somatic cell types than their corresponding colinear isoforms among the ten tissues examined. These results suggest that the expression patterns of *trans*-spliced isoforms do not correlate exactly with those of their corresponding colinear isoforms, despite the latter being a source for the former. Intriguingly, although *RMST* was found to be broadly expressed in the ten tissues examined, expression of ts*RMST* was not detected in these tissues (Fig. 2C; Supplemental Fig. 4). As ts*RMST* is highly expressed in both hESCs and iPSCs and exhibits a step-down in expression after in vitro hESC differentiation, we hypothesize that ts*RMST* may be specifically expressed in pluripotent stem cells and may thus play a role in pluripotency maintenance.

Disruption of ts*RMST* expression impairs pluripotency maintenance

To explore the functional role of ts*RMST* in pluripotency maintenance of hESCs, we disrupted ts*RMST* expression using a small hairpin RNA (shRNA), shTS2, designed to target the chimeric junction site of ts*RMST* into hESCs (Supplemental Fig. 5). We first showed that alkaline phosphatase staining (Supplemental Material) was reduced in these hESCs as compared to hESCs transfected with control virus (shLuc) (Fig. 3A). Microarray-based global gene expression profiling further revealed that the expression levels of pluripotent genes, such as *NANOG*, *POU5F1*, *SOX2*, and *TCF7L1*, were significantly decreased in ts*RMST* knockdown hESCs, whereas key lineage-specific transcription factors, such as *GATA6* (endoderm) and *PAX6* (neuroectoderm), were increased (Fig. 3B). We reexamined mRNAs of hESCs at various time points after shTS2 transduction by qRT-PCR; this revealed that ts*RMST* knockdown did indeed result in a significant decrease in pluripotent gene expression (*NANOG*, *POU5F1*, *SOX2*, and *TCF7L1*) but an increase in the expression of mesodermal genes (*T*, *MIXL1*, and *GSC*), endodermal genes (*GATA4*, *GATA6*, *SOX7* and *SOX17*), and neuroectoderm genes (*PAX6* and *SOX1*) (Fig. 3C). To further validate the effect of ts*RMST* knockdown on pluripotency maintenance, we performed fluorescence activated cell sorting (FACS) and immunocytochemical (ICC) analyses (Supplemental Material), which revealed that the expression of the pluripotent markers NANOG and POU5F1 was significantly decreased by transfection of hESCs with shTS2 (Fig. 3D,E). By contrast, the numbers of T^+ (mesoderm) and $SOX17^+$ (endoderm) cells were increased by day 4 after transfection, and the number of $PAX6^+$ (neuroectoderm) cells

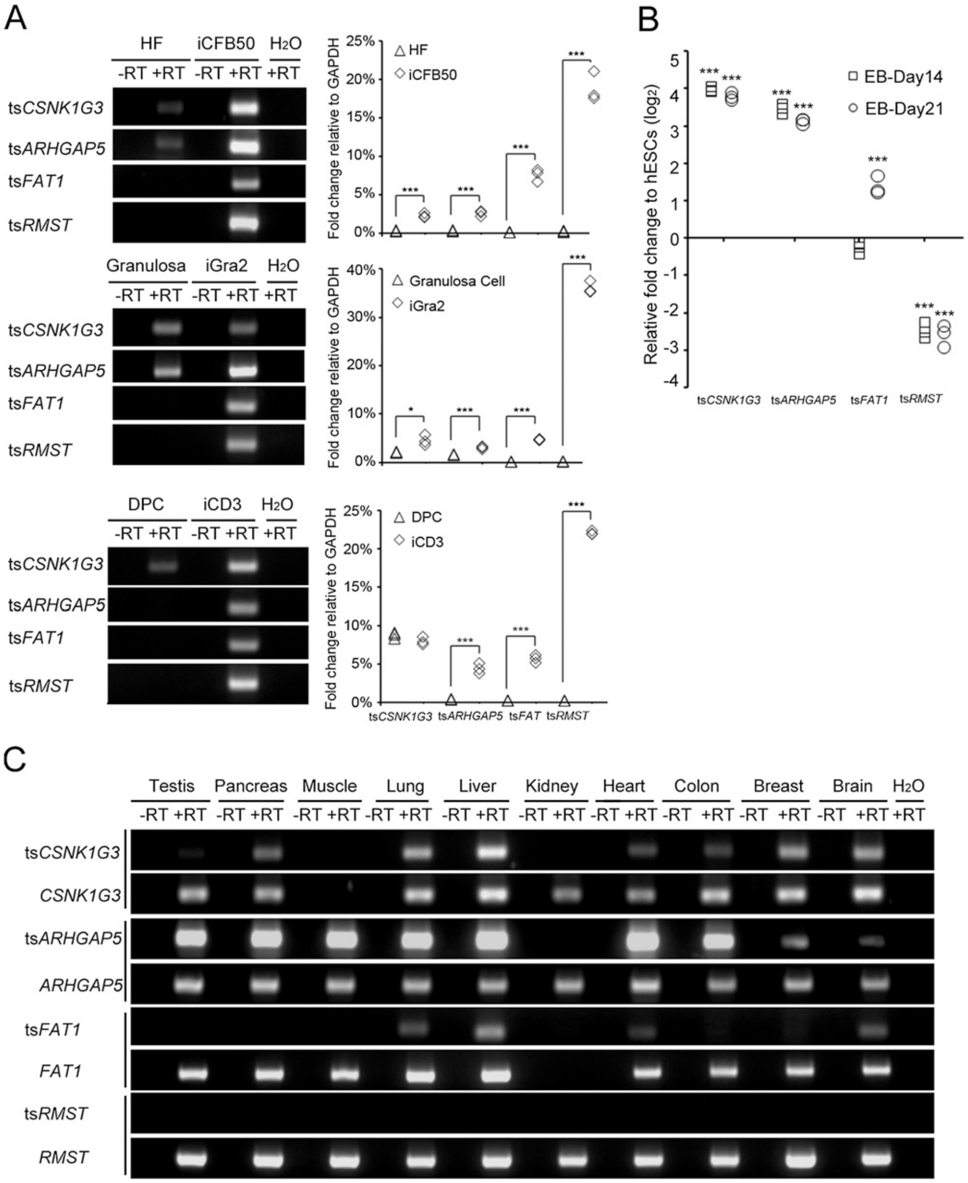

Figure 2. Expression profiles of ts*CSNK1G3*, ts*ARHGAP5*, ts*FAT1*, and ts*RMST* in human pluripotent stem cells and normal tissues. (*A*) RT-PCR and qRT-PCR analysis of ts*CSNK1G3*, ts*ARHGAP5*, ts*FAT1*, and ts*RMST* in iPSCs derived from human foreskin fibroblasts (iCFB50) (Huang et al. 2010), granulosa cells (iGRA2), and dermal papilla cells (iCD3) with their respective parental cell lines. (HF) Human foreskin fibroblasts; (Gra) granulosa cells; (DPC) dermal papilla cells. (*B*) qRT-PCR analysis of ts*CSNK1G3*, ts*ARHGAP5*, ts*FAT1*, and ts*RMST* at various stages of hESC in vitro differentiation (i.e., day 14 and day 21). (*C*) RT-PCR products of the four *trans*-spliced transcripts (ts*CSNK1G3*, ts*ARHGAP5*, ts*FAT1*, and ts*RMST*) and their corresponding colinear isoforms in ten human normal tissues. All *P*-values were estimated by the two-sample, two-tailed *t*-test. Significance: (*) $P < 0.05$; (**) $P < 0.01$; and (***) $P < 0.001$.

were increased by day 7 (Fig. 3E). To control for possible off-target effects, we proceeded to rescue shTS2 knockdown by expressing the ts*RMST* transcript in shTS2 virus-infected hESCs (shTS2-rescue) (Supplemental Fig. 5). We showed that the numbers of NANOG^{+} and POU5F1^{+} cells were significantly greater in shTS2-rescued hESCS than in knockdown cells, as revealed by FACS (Fig. 3F) and ICC analysis (Fig. 3G). Furthermore, expression of *NANOG*, *POU5F1*, *TCF7L1*, and *SOX2* was remarkably increased in the shTS2-rescued hESCs, as shown by qRT-PCR (Fig. 3H). The shTS2-rescued hESCs also possessed the typical morphological traits of hESCs and stained strongly for alkaline phosphatase (Fig. 3I). These results thus demonstrate that ts*RMST* indeed plays a functional role in pluripotency maintenance in hESCs.

The ts*RMST* transcript interacts with the pluripotency transcription factor NANOG and the PRC2 complex factor SUZ12

We further investigated the mechanism by which ts*RMST* regulates pluripotency maintenance. Relative ts*RMST* expression in the cytoplasm and nucleus of hESCs were examined by qRT-PCR. We found that ts*RMST* transcripts were highly enriched in the nuclei of hESCs (Fig. 4A), similar to *lncRNA-ES1*, another lincRNA previously reported in hESCs (Ng et al. 2012). As nuclear lincRNAs may act in *cis* to activate gene expression or in *trans* to suppress transcription (Guttman and Rinn 2012), the effects of ts*RMST* on expression of its neighboring genes were investigated (Fig. 4B).

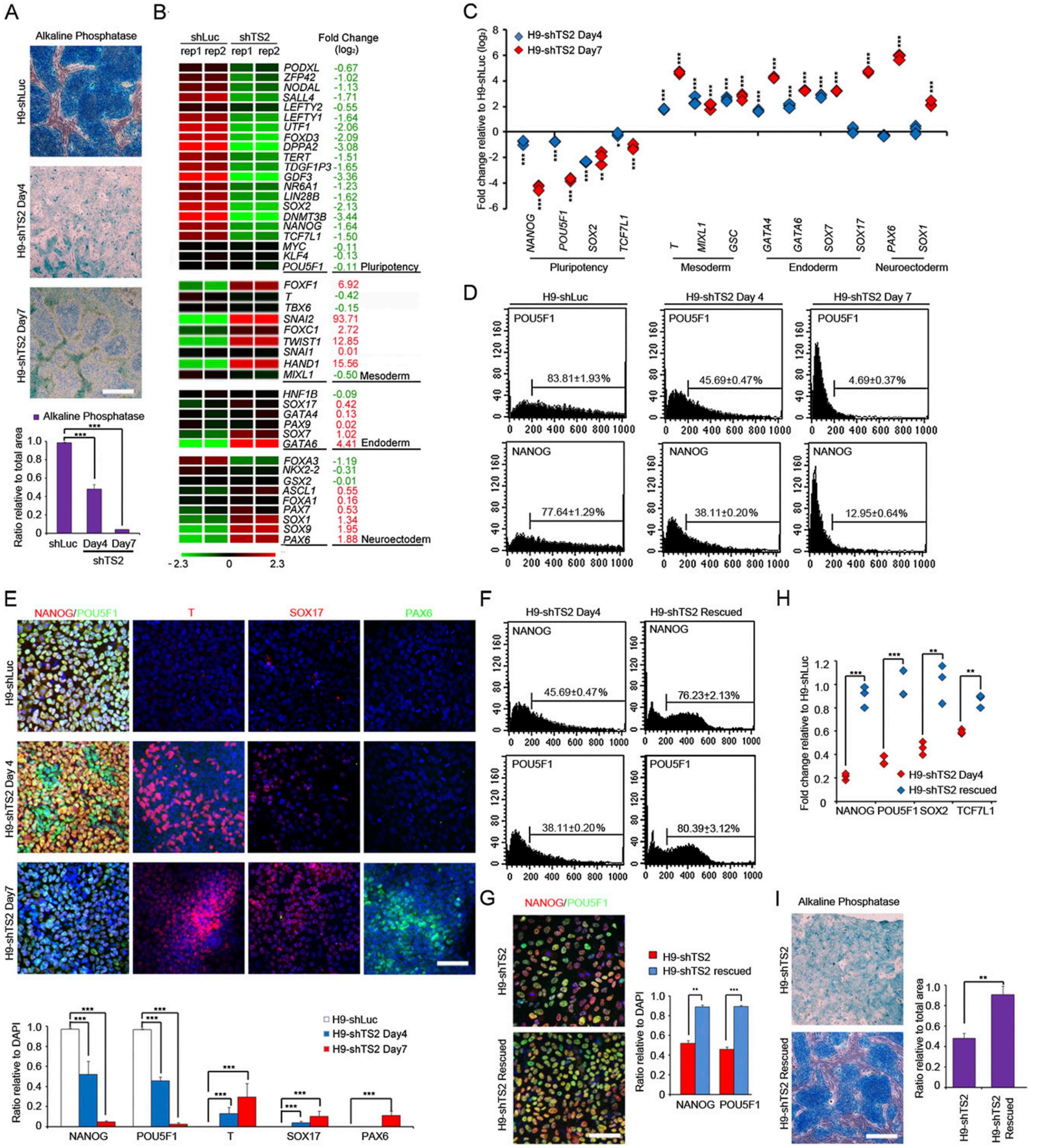

Figure 3. Effect of ts*RMST* knockdown on pluripotency maintenance of hESCs. (*A*) Alkaline phosphatase staining and quantification of hESCs transfected with control (shLuc) or shTS2 virus at 4 and 7 d post-viral transduction. (Scale bar) 200 μm. (*B*) Heat map clustering analysis of genes related to pluripotency, neuroectoderm, mesoderm, and endoderm in shLuc- and shTS2-transduced hESCs. Relative fold changes are listed. Green and red values represent fold change for down- and up-regulation, respectively. (*C*) qRT-PCR analysis of RNA isolated from hESCs transfected with control or shTS2 virus at 4 and 7 d post-viral transduction, to detect pluripotency-related genes (*NANOG*, *POU5F1*, *SOX2*, *TCF7L1*), and lineage-specific genes, including mesodermal markers (*T*, *GSC*, *MIXL1*), endodermal markers (*SOX17*, *GATA4*, *GATA6*, *SOX7*), and neuroectodermal markers (*PAX6*, *SOX1*). (*D*) Fluorescence-activated cell sorting (FACS) analysis of NANOG$^+$ and POU5F1$^+$ cell populations in hESCs transfected with shLuc or shTS2 virus at 4 and 7 d post-viral transduction. Three independent transfections were performed to determine the mean. (*E*) Immunocytochemistry analysis and quantification of the expression of NANOG, POU5F1 (pluripotency markers), T (mesodermal marker), SOX17 (endodermal marker), and PAX6 (ectodermal marker) in shTS2-transduced hESCs at 4 and 7 d post-viral transduction. (Scale bar) 20 μm. (*F*) FACS analysis of NANOG$^+$ and POU5F1$^+$ cell populations in shTS2 virus-transfected hESCs and shTS2-rescue hESCs. Three independent transfections were performed to determine the mean. (*G*) Immunocytochemistry analysis and quantification of the expression of NANOG and POU5F1 (pluripotency markers) in shTS2 virus-transfected hESCs and shTS2-rescue hESCs. (Scale bar) 20 μm. (*H*) qRT-PCR analysis of pluripotency-related genes (*POU5F1*, *NAONG*, *SOX2*, *TCF7L1*) in RNA isolated from shTS2 virus-transfected and shTS2-rescue hESCs. (*I*) Alkaline phosphatase staining and quantification of shTS2 virus-transfected hESCs with or without ts*RMST* coexpression (shTS2-rescue). (Scale bar) 200 μm. All indicated *P*-values were estimated by the two-tailed two-sample *t*-test. Significance: (*) $P < 0.05$; (**) $P < 0.01$; and (***) $P < 0.001$.

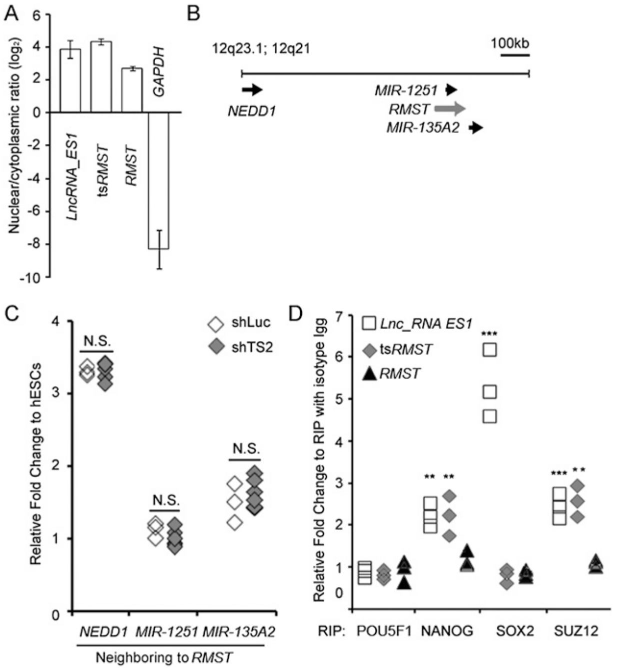

Figure 4. Investigation of the mechanism by which ts*RMST* regulates pluripotency maintenance and early lineage differentiation. (*A*) The nuclear to cytoplasmic expression ratio of *RMST*, ts*RMST*, *lncRNA-ES1*, and *GAPDH* in hESCs. Error bars represent the mean values ± one standard deviation. (*B*) Neighboring genes (*NEDD1*) and miRNAs (*MIR1251* and *MIR135A2*) of ts*RMST* within a 1-MB window on chromosome 12q based on the UCSC annotation. Arrowheads indicate the transcriptional orientations of genes or miRNAs. (*C*) qRT-PCR analysis of *NEDD1*, *MIR1251*, and *MIR135A2* on hESCs transfected with control shLuc and shTS2 lentivirus. (*D*) RIP assays of ts*RMST*, *RMST*, and *lncRNA-ES1* using antibodies against POU5F1, SOX2, NANOG, and the PRC2 component factor SUZ12 in hESCs. The RIP enrichments of ts*RMST*, *RMST*, and *lncRNA-ES1* were measured by qRT-PCR, and each value was normalized to the level of background RIP detected for an isotype IgG. *P*-values were estimated by the two-tailed two-sample *t*-test. Significance: (*) $P < 0.05$; (**) $P < 0.01$; and (***) $P < 0.001$. (N.S.) Not significant.

Knockdown of ts*RMST* did not affect expression of the genes and microRNAs located within a 1-MB range of ts*RMST* (which include *NEDD1*, *MIR1251*, and *MIR135A2*), suggesting that ts*RMST* does not act in *cis* to regulate expression of its neighbors (Fig. 4C). Next, we examined whether ts*RMST* controls pluripotency by acting in *trans*. As pluripotency-associated lincRNAs have been shown to bind pluripotency-related transcription factors and recruit the chromatin modifier (i.e., the PRC2 complex) to suppress target gene expression in hESCs (Ng et al. 2012), we investigated whether ts*RMST* controls hESC pluripotency and/or lineage differentiation through a similar mechanism. We performed RNA immunoprecipitation (RIP) assays (Supplemental Material), in which cross-linked RNA-protein complexes were immunoprecipitated with antibodies against SUZ12 (a component of the PRC2 complex) and three pluripotency-related transcription factors (POU5F1, NANOG, and SOX2). RIP enrichment (as measured by qRT-PCR) indicated that ts*RMST* interacts with SUZ12 and NANOG (Fig. 4D). By examining the ENCODE ChIP-seq data (The ENCODE Project Consortium 2012), we found that the number of genes occupied by both SUZ12 and NANOG in hESCs was significantly larger than expected (O/E ratio [observed-to-expected ratio] = 1.19, *P*-value < 10^{-15} by the χ^2 test) (Fig. 5A). Ingenuity Pathway Analysis further revealed that the genes occupied by both NANOG and SUZ12 were significantly enriched in the two pathways: transcriptional regulatory network in ESCs and role of POU5F1 in mammalian ESC pluripotency (both *P*-values < 0.001) (Fig. 5B; Supplemental Table 1). These results thus suggest that ts*RMST* may control pluripotency via mediating the recruitment of the PRC2 complex (which mediates the H3K27me3 modification) to silence a specific set of NANOG-targeted genes in hESCs. Intriguingly, we found that the ts*RMST* repressed lineage-specific genes, *GATA4*, *GATA6*, and *PAX6*, (Fig. 3B,C), were also bound by both NANOG and SUZ12 (Supplemental Table 1). Thus, we proceeded to use ChIP-qPCR to confirm that ts*RMST* knockdown in hESCs reduced NANOG and SUZ12 occupancy and the H3K27me3 modification on the *GATA4*, *GATA6*, and *PAX6* promoters (Fig. 5C–E). Together, these results indicate that ts*RMST* may contribute to pluripotency maintenance of hESCs by suppressing lineage-specific gene expression via the recruitment of NANOG and the PRC2 complex.

Discussion

To the best of our knowledge, this is the first study to investigate *trans*-splicing in hESCs. The integrative transcriptome sequencing approach used was found to be a powerful approach for minimizing potential false positives while detecting *trans*-splicing. With the application of TSscan screening, we observed that only a small number of *trans*-splicing candidates were simultaneously supported by different NGS data sets; thus the events ultimately identified by TSscan only represent ~0.1% (9/8,822) of the 454-nominated candidates generated (Fig. 1A). Three possible scenarios may account for this result: (1) There is considerable sequence diversity (or individual polymorphism) between H1 and H9 hESC lines; (2) *trans*-spliced RNAs tend to be expressed at a very low level in hESCs and are therefore not easily detected between multiple NGS data sets; or (3) most of the TSscan-excluded cases represent experimental artifacts. The first scenario is unlikely because if we consider the candidates inferred from the NGS of the same hESC line, <0.1% of the 454-nominated candidates were also supported by Illumina reads (20/2511 in S1) or SOLiD reads (4/6312 in S4) (see Fig. 1B). On the other hand, we found that a considerable number of candidates (681/8822) were supported by at least two 454-reads (31 were even supported by five or more reads), which were not detected by any Illumina/SOLiD reads. Of note, the Illumina/SOLiD platforms normally generate RNA-seq reads in much greater quantities than the 454 platform (Metzker 2010; see also Table 1). Thus, the second scenario is also unlikely because a considerable number of candidates were repeatedly detected by the 454 platform but not the Illumina/SOLiD platforms. The presence of experimental artifacts (i.e., the third scenario) is, therefore, the most likely explanation for these platform-dependent cases, consonant with earlier suggestions that experimental artifacts are the most critical issue in *trans*-splicing detection (McManus et al. 2010; Ozsolak and Milos 2011). This result also highlights the power of TSscan for removing experimental artifacts.

We also observed a considerable number of 454-nominated *trans*-splicing candidates involving sense–antisense (4034 cases; 47.1%) or mitochondrial-nuclear gene (2935 cases; 33.2%) fusions. Regarding the former, it has been shown that mRNA and cDNA can become "template partners" and form an artificial sense–antisense in vitro RNA fusion during RT-PCR (Houseley and Tollervey 2010). To examine this possibility, we took a closer look at the 454-nominated candidates with sense–antisense fusions (187 cases) (Supplemental Table 2), in which both the sense and antisense parts came from well-annotated transcripts, and included at least

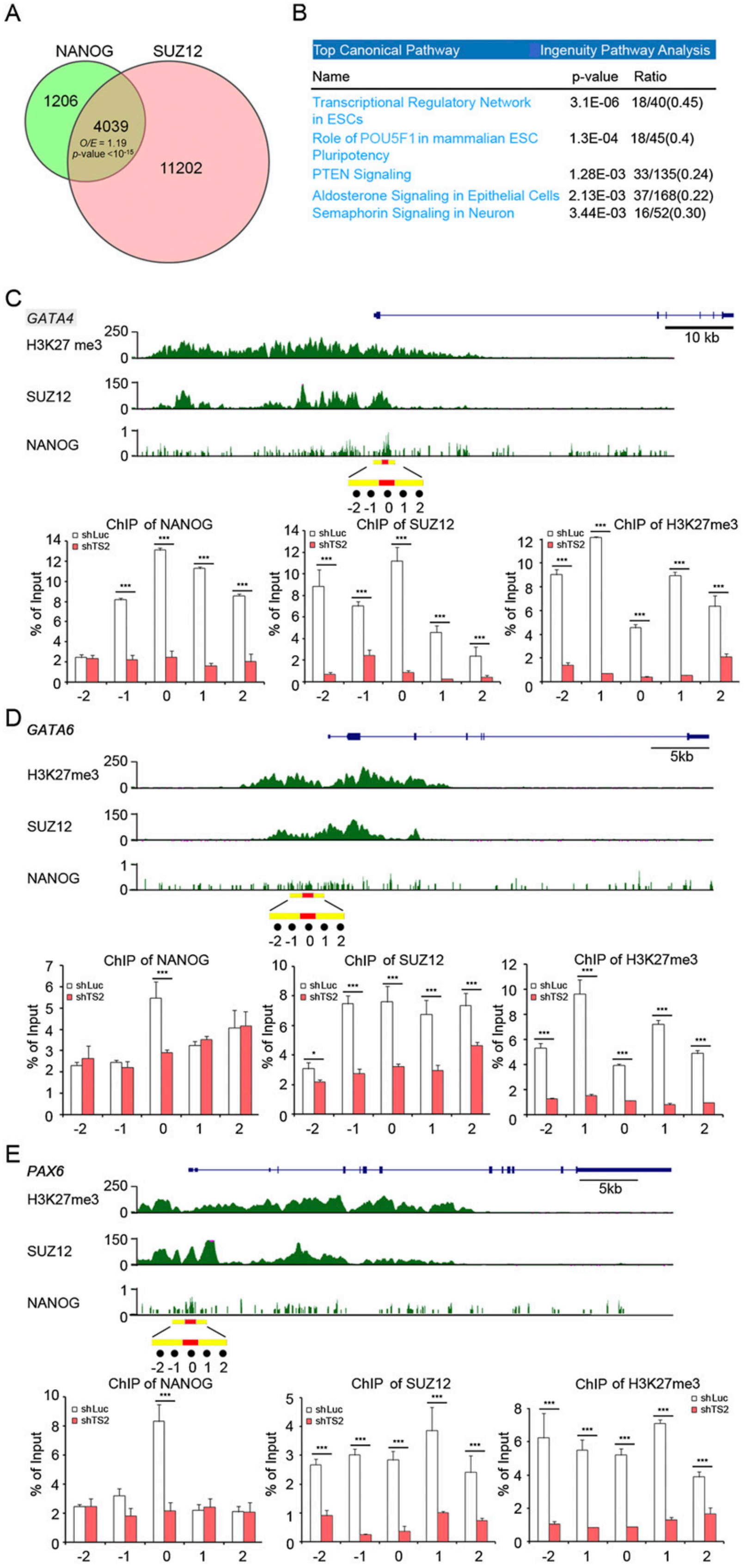

Figure 5. (Legend on next page)

two exons with at least one well-annotated exon–intron boundary. We examined the exon–intron boundaries of these 187 fusion events and the corresponding splicing sites in the genomic sequences. Only three events were found to fulfill the criteria of canonical splicing signals (an example is illustrated in Supplemental Fig. 6A), whereas 143 events (76%) were found to represent apparent experimental artifacts of template switching, in which a spurious RNA contained the canonical splicing site, "GT-AG," in one part of the fusion and a noncanonical splicing site such as "CA-TC" in the other part with the opposite strand (as illustrated in Supplemental Fig. 6B). However, the authenticity of even the sense–antisense RNA fusions (which fulfill the criteria of canonical splicing signals) remains questionable. The three extracted canonical sense–antisense fusions may still be false positives, because they are not supported by any short Illumina/SOLiD reads examined, and are 454-platform-dependent. These results reveal that most of the sense–antisense fusion candidates nominated by the NGS data are likely to be the result of in vitro artifacts.

It was also shown that mitochondrial-nuclear gene fusions may arise from spontaneous de novo transfer of mtDNAs into the nucleus; the resulting fusion sequences may then be transcribed as part of the transcriptome (Martin 2003). However, mitochondrial-nuclear fusion events that result from genetic arrangements would not occur post-transcriptionally (i.e., they are not *trans*-splicing events). When the 2935 mitochondrial-nuclear fusion events were further examined, only eight were found to be supported by both long and short NGS reads (i.e., four in S1 and four in S3) (see Supplemental Table 3). These results suggest that most of the 454-supported mitochondrial-nuclear events are experiment-dependent and likely to be experimental artifacts. Moreover, even the four mitochondrial-nuclear candidates supported by both long and short reads from H1 and H9 ESCs (belonging to S3) failed AMV-based RT-PCR validation (Supplemental Fig. 7). Therefore, we conclude that the observed mitochondrial-nuclear fusions are likely to be in vitro artifacts and thereby excluded by TSscan (Step 3) (Fig. 1A). These results are reminiscent of those of previous NGS-based studies, which regarded mitochondrial-nuclear fusions as false positives and directly excluded them when detecting gene fusions (Maher et al. 2009b; McManus et al. 2010).

Similar to an earlier report (McManus et al. 2010), we did not obtain credible evidence for the existence of intergenic *trans*-splicing events, although most of the 454-nominated candidates were intergenic (8003/8822) (see Supplemental Table 4). We compared the intergenic with the intragenic candidates (731 cases) (Supplemental Table 4) by the three in silico filters stated above (i.e., SHS-containing, sense-antisense fusion, and mtDNA-containing) (Fig. 1A). Of note, the candidates that were formed in an intrachromosomal fashion and involved nongenic loci (88 cases) were not considered in the comparison. We found that intergenic candidates consist of a significantly higher percentage of SHS-containing candidates, sense–antisense fusion candidates, and mtDNA-containing candidates than the intragenic candidates (all *P*-values < 10^{-15} by the two-tailed Fisher's exact test) (Supplemental Table 4). In addition, chimeric RNA products with canonical splice sites and matching annotated exon boundaries are regarded as being less likely to be generated in vitro (Kim et al. 2010; Al-Balool et al. 2011). We found that the intragenic cases have a significantly higher percentage of candidates with canonical splice sites and matching annotated exon boundaries than the intergenic ones (*P*-value < 10^{-13}) (Supplemental Table 4). These observations further suggest that most intergenic candidates arise from experimental artifacts rather than *trans*-splicing.

Several methods/pipelines have been developed to identify chimeric RNAs formed from cancer-related mutations, and these use RNA-seq data derived from a single NGS platform, e.g., TopHat-Fusion (Kim and Salzberg 2011), FusionSeq (Sboner et al. 2010), FusionHunter (Li et al. 2011), ChimeraScan (Iyer et al. 2011), FusionFinder (Francis et al. 2012), Bellerophontes (Abate et al. 2012), and SOAPfuse (Jia et al. 2013). These methods may also be used to detect *trans*-splicing candidates. However, although the use of a single NGS platform is more economical and practical, it was reported that sequencing with various platforms results in a very low level of overlap for chimeric RNAs (Maher et al. 2009a) and that almost no overlap was observed among different single-platform-based tools (Nacu et al. 2011; Abate et al. 2012; Carrara et al. 2013a,b), with the outcome that the majority of predicted chimeric RNAs are likely to be false positives. Integrating long- and short-read sequence data can overcome the limitations inherent in both systems (namely, the potential for false positives arising from lack of depth in long reads and the possibility of mapping errors in short reads) (Maher et al. 2009a); as such, we used such an integrative approach to investigate novel *trans*-splicing events. In addition, currently available methods for detecting chimeric RNAs are generally unable to distinguish *trans*-splicing events from genetic rearrangements. We thus emphasize the unique advantage of our pipeline, in that it simultaneously accounts for possible experimental artifacts and genetic rearrangements.

To confirm the *trans*-splicing candidates identified by TSscan, we performed multiple-step validations to rule out potential RTase-based artifacts (using comparisons of two different RTase products and a non-RTase-based validation [RPA]) in multiple hESC lines. There are four observations of note. First, RT-PCR assays using the same RTase for two independent cDNA preparations are not sufficient to exclude template switching events. Second, the number of supported RNA-seq reads cannot indicate whether a chimeric RNA product is an artifact, because certain chimeric RNA products that were unsupported by experimental validation had a greater number of supported RNA-seq reads than validated ones (Table 2). This is also consistent with the earlier observation that experimental artifacts can emerge repeatedly during reverse transcription (Houseley and Tollervey 2010; McManus et al. 2010). Third, the presence of canonical splicing signals does not guarantee that a *trans*-splicing candidate is genuine. For example, ts*SOBP* contains canonical splicing signals at its chimeric junction sites, but was not validated experimentally (Fig. 1D; Supplemental Fig. 2). The conclusions of earlier reports that did not detect template switching in *trans*-spliced RNA with canonical splicing signals at their chimeric junction sites (Cocquet et al. 2006; Al-Balool et al. 2011) thus need to be reevaluated. Finally, *trans*-splicing candidates nominated by different types of NGS data appear to include different proportions of in vitro artifacts. For example, SOLiD-supported candidates appear to be less likely to be experimental artifacts than Illumina-supported candidates (Table 1). A possible reason for this discrepancy is that these two NGS platforms use different approaches to prepare the transcriptome libraries (Supplemental Discussion), further suggesting that an integrative transcriptome sequencing approach is advantageous in detecting *trans*-splicing events. In addition, we found that the validated event supported by both types of NGS data (i.e., ts*RMST*) had similar read coverage levels using both the Illumina and SOLiD system (see Supplemental Table 5), also supporting the preceding hypothesis that read coverage level is not a reliable indicator of experimental artifact rates.

Figure 5. Knockdown of ts*RMST* in hESCs decreased the H3K27me modification on the promoters of NANOG and SUZ12 occupied genes. (*A*) Venn diagram and the observed-to-expected (O/E) ratio of genes bound by both NANOG and SUZ12. The total number of analyzed genes was 23,671. *P*-value was estimated by the χ^2 test. The ChIP-seq data of NANOG and SUZ12 were generated by the ENCODE project (The ENCODE Project Consortium 2012) and downloaded from the UCSC Genome Browser at http://genome.ucsc.edu/. A NANOG-/SUZ12-occupied gene was defined by the binding of NANOG/SUZ12 to its promoter region, centered within 2000 bp of the transcription start site. (*B*) Top five canonical pathways for the genes bound by both NANOG and SUZ12, as determined by Ingenuity Pathway Analysis (IPA) (Supplemental Table 1). The ratios represent the number of genes bound by both NANOG and SUZ12 divided by the total number of genes within the corresponding pathway. (*C–E*) ChIP-qPCR analysis of the H3K27me3 modification and the occupancy of NANOG and SUZ12 on the promoters of three lineage-specific genes repressed by ts*RMST*. (*C*) *GATA4* (chr8:11565365−11617509); (*D*) *GATA6* (chr18:19749416−19782227); and (*E*) *PAX6* (chr11:31806340−31832879). ENCODE ChIP-seq data of NANOG and SUZ12 occupancy and the H3K27me3 modification were aligned to the promoter regions of the lineage-specific genes, as indicated. The promoter regions were defined as −2 kb to +2 kb of the transcription start sites. For each figure, the *y*-axis of the *upper* panel represents the intensity of ChIP-seq reads. The highest NANOG binding peaks on the promoter regions of *GATA4*, *GATA6*, and *PAX6* were highlighted with red bars (chr8:11567094–11567723 for *GATA4*, chr18:19747482–19747800 for *GATA6*, and chr11:31832538–31832842 for *PAX6*). ChIP fragments containing the selected NANOG binding peak (labeled as 0) or its four flanking regions (labeled as −1, −2, 1, and 2, which were located within −1 kb to +1 kb of the selected NANOG binding peak [highlighted with yellow bars]) in shLuc and shTS2 transduced hESCs were quantified by qPCR, and respectively normalized with the input genome used in ChIP. The same process was applied to SUZ12 and H3K27me3. The primers are listed in Supplemental Table 6.

In this study, four *trans*-splicing events (ts*CSNK1G3*, ts*ARHGAP5*, ts*FAT1*, and ts*RMST*) were identified and experimentally confirmed in hESCs. These events have not been previously identified in ESCs, and ts*RMST* is the first reported *trans*-spliced lincRNA. We have shown that these events are all highly expressed in human pluripotent stem cells (hESCs/iPSCs) (Figs. 1C–E, 2A) and differentially expressed during the pluripotent-to-differentiation transition (Fig. 2B), suggesting their potential biological significance in pluripotency and/or early lineage differentiation. By performing ts*RMST* knockdown and a series of careful experimental validations (including alkaline phosphatase staining, microarray analysis, qRT-PCR, FACS, ICC, and cDNA rescue) (Fig. 3), we further confirmed that ts*RMST* was significantly associated with the pluripotency maintenance of hESCs. We have provided evidence that ts*RMST* does not act in *cis* to regulate expression of its neighbors (Fig. 4C), but can interact with a key pluripotency transcription factor, NANOG, as well as the PRC2 component, SUZ12, to control pluripotency in *trans* through silencing NANOG target and/or lineage-specific genes in hESCs by recruiting the suppressive PRC2 complex (Fig. 4D). Indeed, analysis of ENCODE ChIP-seq data revealed that SUZ12 was enriched in the promoter region of NANOG-binding genes (Fig. 5A). ChIP-qPCR experiments on the promoters of the ts*RMST* repressed lineage-specific genes (*GATA4*, *GATA6*, and *PAX6*) further showed the loss of NANOG and SUZ12 occupancy and H3K27me3 modification in ts*RMST* knockdown hESCs (Fig. 5C–E). Accordingly, we propose a putative model in which ts*RMST* suppresses lineage differentiation in hESCs via the recruitment of NANOG and the PRC2 complex (Fig. 6). Our findings accord with a recent report that lincRNAs are important regulators of pluripotency (Ng et al. 2012), and as such, ts*RMST* may be a novel pluripotency-related lincRNA.

Recent reports have indicated that circular RNAs may be abundant for some human genes (Salzman et al. 2012; Jeck et al. 2013), and it was therefore possible that the identified *trans*-splicing events shared chimeric junction sites with circular RNAs. Our search of the literature suggests that these events have not been previously identified as circular RNAs. To experimentally examine if some or all of these events represented circular RNAs, we treated total RNA with RNase R, which degrades linear RNA alone (Supplemental Material). The qRT-PCR analysis showed that, for all four chimeric RNAs, the overwhelming majority of the transcripts were degraded by RNase R in multiple hESC lines (H1, H9, and NTU1) (Supplemental Fig. 8). We have thus demonstrated that the chimeric events identified by this study are indeed *trans*-spliced RNAs.

In conclusion, our results highlight the potential of integrative analysis of high-throughput transcriptome sequencing data derived from multiple platforms and cell lines to minimize potential false positives (particularly experimental artifacts) while identifying *trans*-spliced transcripts. Our findings also provide important insights into the role of *trans*-splicing in the pluripotency maintenance of hESCs and lineage differentiation. This study thus establishes a potentially valuable pipeline for comprehensive and rigorous characterization of *trans*-splicing, expanding the discovery of this important but understudied class of post-transcriptional events.

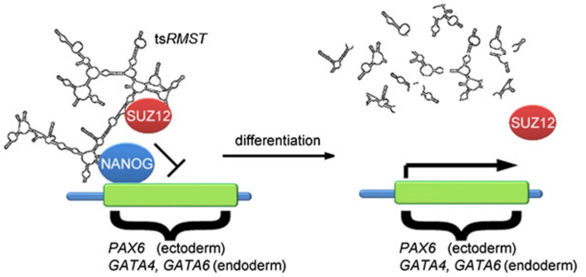

Figure 6. A putative model for regulation of gene expression by ts*RMST* in pluripotent stem cells.

Methods

The TSscan pipeline

The TSscan pipeline is made up of four main steps (Fig. 1A). First, all 454-reads were aligned against the human reference genome (GRCh37) using BLAT with default parameters (Kent 2002). Each extracted chimeric alignment is composed of two topologically distinct mapped parts (or two tandem duplications), which may include an overlap (i.e., SHSs) or gap between the two parts. Both of the nonoverlapping regions of the mapped parts had to be > 50 bp with ≥ 95% sequence identity to the reference genome. A chimeric RNA candidate had to satisfy two criteria: In the BLAT result, the two mapped parts of a chimeric alignment had to cover the longest alignable length of the 454-read; and the sum of the alignable length of these two parts had to be ≥ 20 bases longer than any of possible colinear alignments. Subsequently, 8822 chimeric RNA candidates were extracted (Step 1) (Fig. 1A). In the second step, short RNA-seq reads (derived from the Illumina and SOLiD platforms) were aligned against each of the 8822 454-nominated candidates using BFAST with default parameters (Homer et al. 2009). The BFAST indices used were suggested by the original BFAST study (Homer et al. 2009) and downloaded from the BFAST page at http://sourceforge.net/projects/bfast/files/. Only the short reads that spanned the fusion boundary by >10 nucleotides with ≥95% sequence identity on each side of the nonoverlapping region were retained. Moreover, a matched short read was discarded if it satisfied any one of the following criteria: (1) It contained more than one mismatch; (2) it contained insertion(s)/deletion(s); or (3) it also mapped to the human genome or well-annotated transcripts (including the UCSC- and Ensembl-annotated transcripts). In the third step, *trans*-splicing candidates that met any one of the following in silico criteria were removed: (1) candidates with SHSs (or gaps) > 5 nucleotides spanning the fusion boundaries; (2) sense–antisense fusion candidates containing noncanonical splicing sites; and (3) candidates containing sequences from the mitochondrial genome. Finally, only the S2 and S3 candidates supported by both H9 and H1 hESC cell cultures were retained.

Data retrieval and availability

The human genomic sequences, hg19 (or GRCh37), were downloaded from the UCSC Genome Browser (http://genome.ucsc.edu/). The human annotated transcripts were downloaded from the UCSC Genome Browser (RefSeq) and the Ensembl Genome Browser (all cDNAs; release 59) (http://www.ensembl.org/). The H1 hESC transcriptome sequencing data, including long 454-reads and short Illumina reads, were downloaded from the Gene Expression Omnibus (GEO; http://www.ncbi.nlm.nih.gov/geo/) database (accession number GSE20301). The RNA-seq reads (including 454-, Illumina-, and SOLiD-reads) that supported the 8822 chimeric candidates identified are illustrated in Supplemental Table 5. The RT-PCR/qRT-PCR primers used in this study are listed in Supplemental Table 6.

Cell culture

Mouse embryonic fibroblasts (MEFs) were cultured in DMEM supplemented with 10% fetal bovine serum (FBS), 1× nonessential amino acids (NEAA, Invitrogen), 2 mM L-glutamine (Invitrogen), and 1× penicillin/streptomycin (Invitrogen). Human ESCs (H1/H9 [WiCell Bank] and NTU1) (Chen et al. 2007) and iPSCs were grown on MEF feeders (2×10^4 cells/cm^2) in DMEM/F12 media plus 20% Knockout Serum Replacement (Invitrogen) and 4 ng/mL bFGF (Sigma-Aldrich). Human fibroblasts and granulose and dermal papilla cells were cultured in media similar to the MEF media described above. For in vitro differentiation, ESC colonies were dispersed into small clumps using dispase (Sigma-Aldrich; 1 mg/mL for 30 min) and transferred onto ultra-low attachment plates (Corning) for embryoid body (EB) formation. The media was changed daily for 4 d using the same media as for routine hESC cultures. EBs were then transferred onto 0.1% gelatin-coated culture dishes with FBS-containing media for further differentiation. Media was changed every 2 d.

Transcriptome library preparation and 454 sequencing

Total RNA (10 µg) was extracted from hESC H9 using TRI Reagent (Ambion), and mRNA was purified using a Poly(A) Purist MAG kit (Ambion). One microgram of mRNA was used to synthesize first-strand cDNA using oligo-dT primers provided by the Creator SMART cDNA library Construction Kit (Clonetech). Double-stranded cDNA was then generated from a single-strand cDNA solution by PCR, using primers provided by the manufacturer. Double-stranded cDNA (5 µg) was fragmented by nebulization and used as templates for sequencing. DNA sequencing and data processing were performed by Mission Biotech using a Genome Sequencer GS FLX Titanium System (Roche).

Transcriptome library preparation and SOLiD sequencing

Total RNA (10 µg) was harvested from H9 hESCs using TRI reagent (Ambion) for cDNA library preparation. Enrichment of mRNA by depletion of ribosomal RNA was performed using a RiboMinus transcriptome isolation kit (Invitrogen). RiboMinus RNA (1 µg) was then fragmented using RNase III for 10 min and cleaned up using a RiboMinus concentration module (Invitrogen). Fragmented RNA was ligated with SOLiD adaptor A and reverse transcribed using ArrayScript RT. Products were purified using a MinElute PCR purification kit (Qiagen) and size-selected on a 6% TBE-urea gel. A cDNA library of an appropriate size was amplified using a SOLiD PCR kit. To prepare the sequencing template, the size selected cDNA library was coupled with SOLiD P1 DNA beads, and mixed with an emulsion PCR mixture using a ULTRA-TURRAX tube drive (IKA). Emulsion PCR was performed using a GeneAmp PCR system 9700 according to the manufacturer's program. Templates on SOLiD P1 DNA beads amplified by emulsion PCR were washed, denatured, and enriched using SOLiD P2 bead incubation steps. The enriched templates were then modified at the 3′ end with bead linkers by a terminal transferase reaction and washed and deposited onto SOLiD slides. Sequencing of templates was performed using a SOLiD 3 system and processed with the SOLiD analysis tool pipeline.

RNA isolation, RT-PCR, and qRT-PCR

Total RNA isolated using TRI Reagent (Applied Biosystems) was treated with DNase I (NEB) to remove genomic DNA contamination and then reverse transcribed using an AMV-derived transcriptase (if not otherwise specified) to generate a cDNA library. All RT-PCR products were amplified under 35 cycles using GoTag MasterMix (Promega), and qRT-PCR assays were performed using the KAPA SYBR fast kit (KAPA Biosystems). All primers used are listed in Supplemental Table 6. All qRT-PCR reactions were performed in triplicate.

Microarray analysis

Total RNA (10 µg) purified by TRI reagent (Applied Biosystems) was used to generate biotin-labeled cRNA probes, which were then hybridized to an Affymetrix Human Genome Plus 2.0 Array (Affymetrix). Probe signal intensities were detected using an Affymetrix GeneChip Scanner 7G and analyzed using GeneSpring XI software (Agilent). Pearson centered complete clustering was applied to genes with a fold-change > $2^{\pm 1.5}$ and a P-value < 0.05.

Lentivirus-mediated gene expression and short hairpin RNA knockdown

The ts*RMST* transcript was cloned from the hESC H9 cDNA library and subcloned into lentiviral plasmid FUW with restriction enzymes EcoRI and XbaI. The lentiviral plasmid pLKO_1 (U6p-shRNA) was obtained from the National RNAi Core Facility (Taipei, Taiwan) and construction of a ts*RMST*-targeted shRNA was performed according to a protocol provided by the same facility. Targeting sequences are listed in Supplemental Table 6.

Data access

The H9 hESC transcriptome sequencing data (including long 454-reads and short SOLiD reads) and microarray data generated in the present study have been submitted to the NCBI Gene Expression Omnibus (GEO; http://www.ncbi.nlm.nih.gov/geo/) under accession numbers GSE30557 and GSE32503, respectively. The related in-house programs and document are publicly accessible from our website (http://idv.sinica.edu.tw/trees/TSscan/TSscan.html) or github (https://github.com/TreesLab/TSscan).

Acknowledgments

This work was supported by the Genomics Research Center and Institute of Cellular and Organismic Biology, Academia Sinica, Taiwan, and the National Science Council, Taiwan, under contracts NSC99-2628-B-001-008-MY3 (to T.J.C.) and NSC99-3111-B-001-001 (to H.C.K.). The financial support from the Academia Sinica Research Award for Junior Research Investigators and the Wu Ta-Yuo Memorial Award is also gratefully acknowledged. We thank Li-Yuan Hung and Yen-Zho Chen for programming assistance, Ping-Hung Hsieh and Yung-Chieh Chan for experimental assistance, and Drs. Chung-Hsuan Chen, King-Song Jeng, and Tien-Hsien Chang for helpful comments.

References

Abate F, Acquaviva A, Paciello G, Foti C, Ficarra E, Ferrarini A, Delledonne M, Iacobucci I, Soverini S, Martinelli G, et al. 2012. Bellerophontes: An RNA-Seq data analysis framework for chimeric transcripts discovery based on accurate fusion model. *Bioinformatics* **28:** 2114–2121.

Al-Balool HH, Weber D, Liu Y, Wade M, Guleria K, Nam PL, Clayton J, Rowe W, Coxhead J, Irving J, et al. 2011. Post-transcriptional exon shuffling events in humans can be evolutionarily conserved and abundant. *Genome Res* **21:** 1788–1799.

Ben-Dov C, Hartmann B, Lundgren J, Valcarcel J. 2008. Genome-wide analysis of alternative pre-mRNA splicing. *J Biol Chem* **283:** 1229–1233.

Black DL, Grabowski PJ. 2003. Alternative pre-mRNA splicing and neuronal function. *Prog Mol Subcell Biol* **31:** 187–216.

Blencowe BJ. 2006. Alternative splicing: New insights from global analyses. *Cell* **126:** 37–47.

Bracco L, Kearsey J. 2003. The relevance of alternative RNA splicing to pharmacogenomics. *Trends Biotechnol* **21:** 346–353.

Carrara M, Beccuti M, Cavallo F, Donatelli S, Lazzarato F, Cordero F, Calogero RA. 2013a. State of art fusion-finder algorithms are suitable to detect transcription-induced chimeras in normal tissues? *BMC Bioinformatics* **14:** S2.

Carrara M, Beccuti M, Lazzarato F, Cavallo F, Cordero F, Donatelli S, Calogero RA. 2013b. State-of-the-art fusion-finder algorithms sensitivity and specificity. *BioMed Res Int* **2013:** 340620.

Chan AS, Thorner PS, Squire JA, Zielenska M. 2002. Identification of a novel gene *NCRMS* on chromosome 12q21 with differential expression between Rhabdomyosarcoma subtypes. *Oncogene* **21:** 3029–3037.

Chen FC, Chen CJ, Ho JY, Chuang TJ. 2006. Identification and evolutionary analysis of novel exons and alternative splicing events using cross-species EST-to-genome comparisons in human, mouse and rat. *BMC Bioinformatics* **7:** 136.

Chen HF, Kuo HC, Chien CL, Shun CT, Yao YL, Ip PL, Chuang CY, Wang CC, Yang YS, Ho HN. 2007. Derivation, characterization and differentiation of human embryonic stem cells: Comparing serum-containing versus serum-free media and evidence of germ cell differentiation. *Hum Reprod* **22:** 567–577.

Cocquet J, Chong A, Zhang G, Veitia RA. 2006. Reverse transcriptase template switching and false alternative transcripts. *Genomics* **88:** 127–131.

Djebali S, Lagarde J, Kapranov P, Lacroix V, Borel C, Mudge JM, Howald C, Foissac S, Ucla C, Chrast J, et al. 2012. Evidence for transcript networks composed of chimeric RNAs in human cells. *PLoS ONE* **7:** e28213.

Dorn R, Krauss V. 2003. The *modifier of mdg4* locus in *Drosophila*: Functional complexity is resolved by *trans* splicing. *Genetica* **117:** 165–177.

The ENCODE Project Consortium. 2012. An integrated encyclopedia of DNA elements in the human genome. *Nature* 489: 57–74.

Fang W, Wei Y, Kang Y, Landweber LF. 2012. Detection of a common chimeric transcript between human chromosomes 7 and 16. *Biol Direct* **7:** 49.

Francis RW, Thompson-Wicking K, Carter KW, Anderson D, Kees UR, Beesley AH. 2012. FusionFinder: A software tool to identify expressed gene fusion candidates from RNA-Seq data. *PLoS ONE* **7:** e39987.

Frenkel-Morgenstern M, Gorohovski A, Lacroix V, Rogers M, Ibanez K, Boullosa C, Andres Leon E, Ben-Hur A, Valencia A. 2012. ChiTaRS: A database of human, mouse and fruit fly chimeric transcripts and RNA-sequencing data. *Nucleic Acids Res* **41:** D142–D151.

Gingeras TR. 2009. Implications of chimaeric non-co-linear transcripts. *Nature* **461:** 206–211.

Goeke S, Greene EA, Grant PK, Gates MA, Crowner D, Aigaki T, Giniger E. 2003. Alternative splicing of *lola* generates 19 transcription factors controlling axon guidance in *Drosophila*. *Nat Neurosci* **6:** 917–924.

Graveley BR. 2001. Alternative splicing: Increasing diversity in the proteomic world. *Trends Genet* **17:** 100–107.

Guttman M, Rinn JL. 2012. Modular regulatory principles of large non-coding RNAs. *Nature* **482:** 339–346.

Hastings KE. 2005. SL *trans*-splicing: Easy come or easy go? *Trends Genet* **21:** 240–247.

Herai RH, Yamagishi ME. 2010. Detection of human interchromosomal *trans*-splicing in sequence databanks. *Brief Bioinform* **11:** 198–209.

Homer N, Merriman B, Nelson SF. 2009. BFAST: An alignment tool for large scale genome resequencing. *PLoS ONE* **4:** e7767.

Horiuchi T, Aigaki T. 2006. Alternative *trans*-splicing: A novel mode of pre-mRNA processing. *Biol Cell* **98:** 135–140.

Houseley J, Tollervey D. 2010. Apparent non-canonical trans-splicing is generated by reverse transcriptase *in vitro*. *PLoS ONE* **5:** e12271.

Hsu MT, Coca-Prados M. 1979. Electron microscopic evidence for the circular form of RNA in the cytoplasm of eukaryotic cells. *Nature* **280:** 339–340.

Huang YT, Chen FC, Chen CJ, Chen HL, Chuang TJ. 2008. Identification and analysis of ancestral hominoid transcriptome inferred from cross-species transcript and processed pseudogene comparisons. *Genome Res* **18:** 1163–1170.

Huang HP, Yu CY, Chen HF, Chen PH, Chuang CY, Lin SJ, Huang ST, Chan WH, Ueng TH, Ho HN, et al. 2010. Factors from human embryonic stem cell-derived fibroblast-like cells promote topology-dependent hepatic differentiation in primate embryonic and induced pluripotent stem cells. *J Biol Chem* **285:** 33510–33519.

Iyer MK, Chinnaiyan AM, Maher CA. 2011. ChimeraScan: A tool for identifying chimeric transcription in sequencing data. *Bioinformatics* **27:** 2903–2904.

Jeck WR, Sorrentino JA, Wang K, Slevin MK, Burd CE, Liu J, Marzluff WF, Sharpless NE. 2013. Circular RNAs are abundant, conserved, and associated with ALU repeats. *RNA* **19:** 141–157.

Jia W, Qiu K, He M, Song P, Zhou Q, Zhou F, Yu Y, Zhu D, Nickerson ML, Wan S, et al. 2013. SOAPfuse: An algorithm for identifying fusion transcripts from paired-end RNA-Seq data. *Genome Biol* **14:** R12.

Jin L, Kryukov K, Clemente JC, Komiyama T, Suzuki Y, Imanishi T, Ikeo K, Gojobori T. 2008. The evolutionary relationship between gene duplication and alternative splicing. *Gene* **427:** 19–31.

Kent WJ. 2002. BLAT—the BLAST-like alignment tool. *Genome Res* **12:** 656–664.

Kim D, Salzberg SL. 2011. TopHat-Fusion: An algorithm for discovery of novel fusion transcripts. *Genome Biol* **12:** R72.

Kim P, Yoon S, Kim N, Lee S, Ko M, Lee H, Kang H, Kim J. 2010. ChimerDB 2.0–a knowledgebase for fusion genes updated. *Nucleic Acids Res* **38:** D81–D85.

Kong L, Zhang Y, Ye ZQ, Liu XQ, Zhao SQ, Wei L, Gao G. 2007. CPC: Assess the protein-coding potential of transcripts using sequence features and support vector machine. *Nucleic Acids Res* **35:** W345–W349.

Krause M, Hirsh D. 1987. A *trans*-spliced leader sequence on actin mRNA in C. elegans. *Cell* **49:** 753–761.

Lasda EL, Blumenthal T. 2011. Trans-splicing. *Wiley Interdiscip Rev RNA* **2:** 417–434.

Li H, Wang J, Mor G, Sklar J. 2008. A neoplastic gene fusion mimics *trans*-splicing of RNAs in normal human cells. *Science* **321:** 5.

Li X, Zhao L, Jiang H, Wang W. 2009. Short homologous sequences are strongly associated with the generation of chimeric RNAs in eukaryotes. *J Mol Evol* **68:** 56–65.

Li Y, Chien J, Smith DI, Ma J. 2011. FusionHunter: Identifying fusion transcripts in cancer using paired-end RNA-seq. *Bioinformatics* **27:** 1708–1710.

Maher CA, Kumar-Sinha C, Cao X, Kalyana-Sundaram S, Han B, Jing X, Sam L, Barrette T, Palanisamy N, Chinnaiyan AM. 2009a. Transcriptome sequencing to detect gene fusions in cancer. *Nature* **458:** 97–101.

Maher CA, Palanisamy N, Brenner JC, Cao X, Kalyana-Sundaram S, Luo S, Khrebtukova I, Barrette TR, Grasso C, Yu J, et al. 2009b. Chimeric transcript discovery by paired-end transcriptome sequencing. *Proc Natl Acad Sci* **106:** 12353–12358.

Maniatis T, Tasic B. 2002. Alternative pre-mRNA splicing and proteome expansion in metazoans. *Nature* **418:** 236–243.

Martin W. 2003. Gene transfer from organelles to the nucleus: Frequent and in big chunks. *Proc Natl Acad Sci* **100:** 8612–8614.

McManus CJ, Duff MO, Eipper-Mains J, Graveley BR. 2010. Global analysis of *trans*-splicing in *Drosophila*. *Proc Natl Acad Sci* **107:** 12975–12979.

Metzker ML. 2010. Sequencing technologies – the next generation. *Nat Rev Genet* **11:** 31–46.

Mudge JM, Frankish A, Fernandez-Banet J, Alioto T, Derrien T, Howald C, Reymond A, Guigó R, Hubbard T, Harrow J. 2011. The origins, evolution and functional potential of alternative splicing in vertebrates. *Mol Biol Evol* **28:** 2949–2959.

Nacu S, Yuan W, Kan Z, Bhatt D, Rivers CS, Stinson J, Peters BA, Modrusan Z, Jung K, Seshagiri S, et al. 2011. Deep RNA sequencing analysis of readthrough gene fusions in human prostate adenocarcinoma and reference samples. *BMC Med Genomics* **4:** 11.

Ng SY, Johnson R, Stanton LW. 2012. Human long non-coding RNAs promote pluripotency and neuronal differentiation by association with chromatin modifiers and transcription factors. *EMBO J* **31:** 522–533.

Nigro JM, Cho KR, Fearon ER, Kern SE, Ruppert JM, Oliner JD, Kinzler KW, Vogelstein B. 1991. Scrambled exons. *Cell* **64:** 607–613.

Nilsen TW. 2001. Evolutionary origin of SL-addition *trans*-splicing: Still an enigma. *Trends Genet* **17:** 678–680.

Ouhammouch M, Brody EN. 1992. Temperature-dependent template switching during *in vitro* cDNA synthesis by the AMV-reverse transcriptase. *Nucleic Acids Res* **20:** 5443–5450.

Ozsolak F, Milos PM. 2011. RNA sequencing: Advances, challenges and opportunities. *Nat Rev Genet* **12:** 87–98.

Rickman DS, Pflueger D, Moss B, VanDoren VE, Chen CX, de la Taille A, Kuefer R, Tewari AK, Setlur SR, Demichelis F, et al. 2009. SLC45A3-ELK4 is a novel and frequent erythroblast transformation-specific fusion transcript in prostate cancer. *Cancer Res* **69:** 2734–2738.

Salzman J, Gawad C, Wang PL, Lacayo N, Brown PO. 2012. Circular RNAs are the predominant transcript isoform from hundreds of human genes in diverse cell types. *PLoS ONE* **7:** e30733.

Sboner A, Habegger L, Pflueger D, Terry S, Chen DZ, Rozowsky JS, Tewari AK, Kitabayashi N, Moss BJ, Chee MS, et al. 2010. FusionSeq: A modular framework for finding gene fusions by analyzing paired-end RNA-sequencing data. *Genome Biol* **11:** R104.

Schoenfelder S, Clay I, Fraser P. 2010. The transcriptional interactome: Gene expression in 3D. *Curr Opin Genet Dev* **20:** 127–133.

Shao X, Shepelev V, Fedorov A. 2006. Bioinformatic analysis of exon repetition, exon scrambling and *trans*-splicing in humans. *Bioinformatics* **22:** 692–698.

Sutton RE, Boothroyd JC. 1986. Evidence for *trans* splicing in trypanosomes. *Cell* **47:** 527–535.

Wu JQ, Habegger L, Noisa P, Szekely A, Qiu C, Hutchison S, Raha D, Egholm M, Lin H, Weissman S, et al. 2010. Dynamic transcriptomes during neural differentiation of human embryonic stem cells revealed by short, long, and paired-end sequencing. *Proc Natl Acad Sci* **107:** 5254–5259.

Zhang G, Guo G, Hu X, Zhang Y, Li Q, Li R, Zhuang R, Lu Z, He Z, Fang X, et al. 2010. Deep RNA sequencing at single base-pair resolution reveals high complexity of the rice transcriptome. *Genome Res* **20:** 646–654.

Received April 24, 2013; accepted in revised form October 3, 2013.